Conformational Studies of Mono- and Bicyclic Parathyroid Hormone-Related Protein-Derived Agonists†

Dale F. Mierke,*,‡ Stefano Maretto,§ Elisabetta Schievano,§ Dominga DeLuca,§ Alessandro Bisello,|| Stefano Mammi,§ Michael Rosenblatt,|| Evaristo Peggion,§ and Michael Chorev*,||

Department of Pharmacology and Molecular Toxicology, University of Massachusetts Medical School, 55 Lake Avenue North, and Department of Chemistry, Clark University, 950 Main Street, Worcester, Massachusetts 01610, Department of Organic Chemistry, University of Padova, Biopolymer Research Center, Via Marzolo 1, Padova, Italy, and Division of Bone and Mineral Metabolism, Harvard-Thorndike and Charles A. Dana Laboratories, Department of Medicine, Beth Israel Deaconess Medical Center and Harvard Medical School, 330 Brookline Avenue (HIM 944), Boston, Massachusetts 02215

Received April 3, 1997; Revised Manuscript Received June 11, 1997⊗

ABSTRACT: Parathyroid hormone-related protein (PTHrP) is expressed in a wide variety of cells where it acts as an autocrine and/or paracrine factor involved in regulation of cellular growth, differentiation, and embryonic development. It may also play a physiological endocrine role in calcium transport across the placenta or during lactation. The N-terminal portion, PTHrP-(1−34), retains all the calciotropic parathyroid hormone-like activity and is a lead structure for the design of novel, bone anabolic agents for the treatment of bone disorders such as osteoporosis. To characterize the putative bioactive conformation, we have carried out a detailed structural analysis of a series of three conformationally constrained PTHrP-(1−34)-based mono- and bicyclic lactam-containing biologically active analogs: (**I**) [Lys^{13},Asp^{17}]PTHrP-(1−34)NH$_2$; **(II)** [Lys^{26},Asp^{30}]PTHrP-(1−34)NH$_2$, and (**III**) [Lys^{13}, Asp^{17}, Lys^{26}, Asp^{30}]PTHrP-(1−34)NH$_2$. The conformational properties were studied by circular dichroisim, nuclear magnetic resonance spectroscopy, distance geometry calculations, and molecular dynamic simulations in water/trifluoroethanol (TFE) mixtures. The helical content in water of both monocyclic analogs **I** and **II** is ∼22%; that of the bicyclic analog **III** is ∼40%. In 30% TFE, all analogs reached a maximal helical content of 80%, corresponding to 26 or 27 residues out of 34 in a helical conformation. High-resolution structures obtained with 50:50 TFE/water revealed that all three analogs display two helical domains and a hinge region around Gly^{12}-Lys^{13}. The highly potent mono- and bicyclic agonists **I** and **III** display a second hinge around Arg^{19}-Arg^{20} which is shifted to Ser^{14}-Asp^{17} in the weakly potent monocyclic agonist **II**. We suggest that the presence and localization of discrete hinges in the sequence together with the high propensity for helicity of the C-terminal sequence and the enhancement of helical nucleation at the N-terminal sequence are essential for generating a PTH/PTHrP receptor-compatible bioactive conformation.

The sequence homology between parathyroid hormone (PTH),[1] an 84-amino acid peptide hormone, and parathyroid hormone-related protein (PTHrP), containing 141 amino acids, is concentrated at the amino terminus. Eight out of the first 13 residues are identical in the two hormones; beyond position 13, the primary sequences diverge. Despite this sequence divergence, both hormones act through the same PTH/PTHrP receptor, a seven helix transmembrane domain-containing G-protein-coupled receptor. The *in vitro* PTH-like activities and the bone-remodeling activities reside in the first N-terminal 34-amino acid regions of both hormones (*1*).

While PTH, which is produced in the parathyroid gland, is a *bona fide* calciotropic hormone, PTHrP is expressed in a wide variety of cells where it acts as an autocrine and/or paracrine factor involved in regulation of cellular growth and differentiation. It appears to play a key role in the early stages of skeletal development in the embryo. In normal physiology, it appears to facilitate calcium transport across the placenta and during lactation. Secretion of PTHrP by certain tumor cells into the circulation and subsequent interaction with PTH/PTHrP receptors in bone and kidney produce the devastating humoral hypercalcemia of malignancy syndrome (*2, 3*).

Our working hypothesis is that, despite major sequence differences, both PTH and PTHrP assume very similar

† This work was supported, in part, by Grants RO1-DK47940 (to M.R.) and GM54082 (to D.F.M.) from the National Institutes of Health.

* To whom correspondence should be addressed: Division of Bone and Mineral Metabolism, Harvard-Thorndike and Charles A. Dana Laboratories, Department of Medicine, Beth Israel Deaconess Medical Center and Harvard Medical School, 330 Brookline Ave. (HIM 944), Boston, MA 02215. Phone: (617) 667-0901. Fax: (617) 667-4432. E-mail: mchorev@warren.med.harvard.edu (M.C.). To whom correspondence should also be addressed: Department of Chemistry, Clark University, 950 Main St., Worcester, MA 01610. Phone: (508) 793-7220. Fax: (508) 793-8861. E-mail: dmierke@black.clarku.edu (D.F.M.).

‡ University of Massachusetts Medical School and Clark University.

§ University of Padova.

|| Beth Israel Deaconess Medical Center and Harvard Medical School.

⊗ Abstract published in *Advance ACS Abstracts,* August 1, 1997.

[1] Abbreviations: CD, circular dichroism; COSY, correlation spectroscopy; DADD, distance- and angle-driven dynamics; DG, distance geometry; DQF, double-quantum-filtered; FTIR, Fourier transform infrared spectroscopy; MD, molecular dynamics; NMR, nuclear magnetic resonance; NOESY, nuclear Overhauser enhancement spectrometry; PTH, parathyroid hormone; PTHrP, parathyroid hormone-related protein; RP-HPLC, reverse phase high-performance liquid chromatography; TFE, trifluoroethanol; TOCSY, total correlation spectroscopy.

S0006-2960(97)00771-X CCC: $14.00

Table 1: Biological Activities[a] of the Lactam-Bridged PTHrP-(1−34)-Derived Agonists[b] (in Nanomolar)

	PTHrP	[Lys^{13},Asp^{17}] (**I**)	[Lys^{26},Asp^{30}] (**II**)	[Lys^{13},Asp^{17},Lys^{26},Asp^{30}] (**III**)
K_b[c]	1.0 ± 0.05	3.2 ± 0.8	410 ± 180	2.1 ± 0.6
K_m[d]	0.57 ± 0.04	0.17 ± 0.03	19 ± 1	0.22 ± 0.02

[a] Published previously in ref 5. [b] Values are mean ± SEM of three independent experiments performed in triplicate. [c] Competitive inhibition of binding of mono[^{125}I]Nle^{8,18},Tyr^{34}]bPTH-(1−34)NH_2 in Saos-2/B-10 cells. [d] Activation of adenylyl cyclase in Saos-2/B-10 cells.

secondary structures which are indistinguishable with respect to binding to the PTH/PTHrP receptor. Large linear peptides, such as PTH-(1−34) and PTHrP-(1−34), are difficult to crystallize and very flexible and display a large ensemble of different conformations in a dynamic equilibrium when in aqueous solution. Therefore, the biologically relevant conformation is not readily discerned. A common practice undertaken to identify the so-called "bioactive conformation" is to gradually reduce the conformational freedom by transforming linear peptides into bioactive cyclic analogs, thereby eliminating a wide range of otherwise accessible conformations. To this end, we have succeeded in designing highly potent cyclic PTHrP-based agonists (1−34) and antagonists (7−34) employing the (*i*)−(*i* + 4) side chain to side chain lactam bridge cyclization. This modification is known to stabilize helical domains and therefore provide a means of validating the relevance of these domains to the bioactive conformation previously hypothesized on the basis of structure−activity studies, predictive methods, and conformational analyses of linear PTH- and PTHrP-derived peptides.

Previous conformational studies of PTHrP-(7−34)-based mono- and dilactam antagonists employing circular dichroisim (CD), nuclear magnetic resonance (NMR), and distance geometry (DG) calculations provided evidence regarding what may be the relevant PTH/PTHrP bioactive conformation (*4*). There appear to be two helical domains spaning sequences 13−18 and 20−34. The midregion lactam (13−17) is instrumental in nucleating an N-terminal helical domain, whereas the C-terminal lactam (26−30) stabilizes an exisiting helical propensity. The unstructured hinge region centered about Arg^{19} in the midregion lactam-containing PTHrP-(7−34) is thought to play a critical role in yielding an antagonist.

The aim of the present study is to gain insight into the conformational requirements for association to and activation of the PTH/PTHrP receptor. In this report, we extend our conformational analysis studies to the new series of PTHrP-(1−34)-based mono- and dilactam agonists: (**I**) [Lys^{13},Asp^{17}]-PTHrP-(1−34)NH_2, (**II**) [Lys^{26},Asp^{30}]PTHrP-(1−34)NH_2, and (**III**) [Lys^{13},Asp^{17},Lys^{26},Asp^{30}]PTHrP-(1−34)NH_2.

Analogs **I** and **III** containing the lactam bridge between Lys^{13} and Asp^{17} display subnanomolar efficacy (K_m = 0.17 and 0.22 nM, respectively) which exceeds that of the linear parent peptide PTHrP-(1−34)NH_2 (K_m = 0.57 nM), while analog **II** is about 30-fold (K_m = 19 nM) less potent than the linear parent peptide (*5*). CD and two-dimensional NMR measurements in TFE/water mixtures as well as DG and MD calculations were performed. The results obtained are compared with those previously reported for conformational studies of mono- and bicyclic PTHrP-derived antagonists and linear PTH- and PTHrP-derived agonists. Taken together, these data are likely to contribute to the design of novel PTH/PTHrP-related bone anabolic agents which will play an important role in osteoporosis therapy.

MATERIALS AND METHODS

Peptide Synthesis, Purification and Biological Activity. Briefly, solid phase peptide synthesis was carried out by employing Nα-Boc protection and *N*,*N*′-dicyclohexylcarbodiimide/*N*-hydroxybenzotriazole/*N*-methylpyrrolidone chemistry for coupling (for details, see ref 5). Peptides were purified by reverse phase high-performance liquid chromatography (RP-HPLC) and analyzed by analytical RP-HPLC, amino acid analysis, and fast atom bombardment mass spectrometry (*5*). The purity of the peptides exceeded 97%. Table 1 contains previously published biological activities of the lactam-bridged PTHrP-(1−34)NH_2 analogs and the corresponding linear parent peptide (*5*). Receptor binding affinity and efficacy in stimulating adenylyl cyclase were determined in human osteoblast-like Saos-2/B10 cells (*6*).

CD Spectroscopy. Spectra were obtained on a JASCO J-715 spectropolarimeter at room temperature in the wavelength range between 185 and 255 nm using quartz cells with an optical path length of 0.001, 0.005, 0.01, and 0.1 cm. Typically, four to eight spectra were averaged and corrected for peptide content, as determined by quantitative amino acid analysis. Calibration was carried out with ammonium D-camphorsulfonate as specified by the manufacturer. The helical content was determined according to the method of Greenfield and Fasman (*7*).

NMR Spectroscopy and Signal Assignments. The concentration of samples for NMR experiments was 3 mM peptide in a 1:1 (v/v) mixture of TFE-d_3/H_2O (CIL, Cambridge, MA). Spectra were recorded on Bruker AM 400 and AMX 600 spectrometers without spinning at 298 K. Data processing was performed on a Bruker X-32 workstation. All two-dimensional spectra were acquired using the time-proportional phase incrementation method (*8*), collecting 320−640 experiments of 2048 (TOCSY and COSY) and 4096 (NOESY) data points. Prior to Fourier transformation, the time domain data were multiplied by $\pi/2-\pi/3$-shifted squared sine bell or Gaussian window functions in both dimensions and zero-filled to 2048 × 1024 (TOCSY and COSY) or 4096 × 1024 (NOESY) real points. Fifth-order polynomial baseline correction was performed in the F_2 dimension after transformation. DQF-COSY spectra (*9*) were acquired using appropriate phase cycling to suppress rapid pulse artifacts (*10*). In CLEAN-TOCSY spectra (*11*, *12*), obtained with a MLEV-17 spin-locking sequence, the mixing time ranged between 65 and 75 ms, the trim pulses were 2.5 ms, and the spin-lock field strength was 6.2 kHz. NOESY spectra were recorded using mixing times of 200 ms with a 10% random variation of the mixing period to reduce ZQ coherence contributions (*13*). Tetramethylsilane was used as an internal standard.

Structure Calculations. The volumes of the integrated cross-peaks from the NOESY spectra were determined using

the AURELIA software package. The calibration in the amide region was based on sequential NH−NH cross-peaks (set to a distance of 2.8 Å for a cross-peak in a well-defined α-helix). Aliphatic regions required a different calibration based on the cross-peak of two methylene β-protons (set to a distance of 1.8 Å) and the cross-peak between α- and β-protons of an alanine residue (set to a distance of 2.1 Å). The resulting distances were then placed into one of four different classes, with upper limits of 2.8, 3.2, 3.5, and 4.0 Å, respectively. In cases where a stereospecific assignment was not possible, the upper distances were further relaxed by the appropriate pseudoatom correction (*14*), yielding two classes of 5.0 and 6.0 Å. The resulting distances were used as upper limits in the distance geometry calculations, while the lower limit was 1.8 Å in all cases.

The distance geometry calculations were carried out with a home-written program utilizing the random metrization algorithm of Havel (*15*), run on Silicon Graphics (R5000) workstations. Experimentally determined distances, more restrictive than the geometric distance bounds (holonomic restraints) (*16*), were added to create a distance matrix. The structures were first embedded in four dimensions and then partially minimized using conjugate gradients followed by distance- and angle-driven dynamics (DADD) (*17*, *18*). The DADD simulation was carried out at 500 K for 100 ps, and then the temperature was gradually reduced to 1 K over the next 40 ps. The DADD procedure utilizes the holonomic and experimental distance restraints plus a chiral penalty function for the generation of the violation "energy" and forces. The resulting structures were then reduced to three dimensions using metrization and the optimization and DADD procedures repeated. Analyses of the structures in terms of NOE violations, order parameter values, and dihedral angle distribution were performed using home-written programs.

The molecular dynamics simulations were carried out using the Discover force field within the Insight II suite of programs (Biosym/MSI Inc.). The structure with the lowest penalty violation from the DG calculations was chosen as the starting structure. The structure was placed in a periodic simulation cell of trifluoroethanol with dimensions of 60, 50, and 50 Å. All solvent molecules within 2.5 Å of the peptide were removed, resulting in 1093, 1094, and 1091 solvent molecules for the simulation of analogs **I**−**III**, respectively. All potential energy parameters for TFE were taken from De Loof et al. (*19*). After solvation, the system was relaxed by energy minimization, consisting of steepest descent and conjugant gradient minimization, first with position restraining of the peptide, followed by energy minimization with all atoms free to move. The temperature of the system was slowly increased to 300 K in 50 K increments for a duration of 1 ps at each temperature. An equilibration period of 10 ps preceded the 120 ps simulation. The NOE restraints, as described above for the DG calculations, were applied throughout the simulation with a force constant of 100 kcal/mol.

RESULTS

CD Measurements. The CD spectra of the three peptides in aqueous solution are concentration- and pH-independent in the range of 10^{-3}−10^{-5} M and pH 3.5−9.0, respectively (data not shown). Analogs **I** and **II** exhibit CD spectra with a similar shape and an estimated helix content of ∼22%,

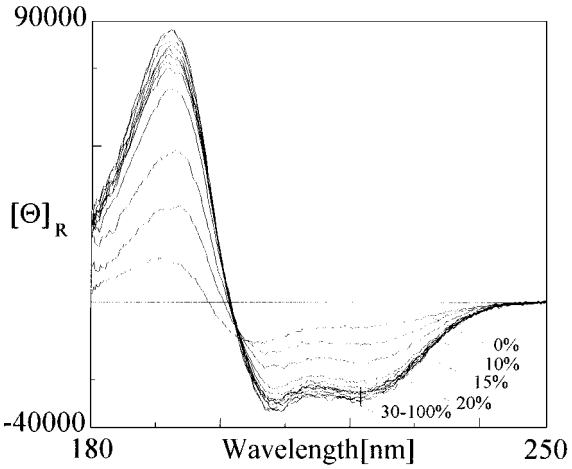

FIGURE 1: CD spectra of analog **I** (12 μM) in a TFE/water solution at various TFE concentrations (v/v indicated). The shift of the 208 nm absorption band is evident for the 100% water solution.

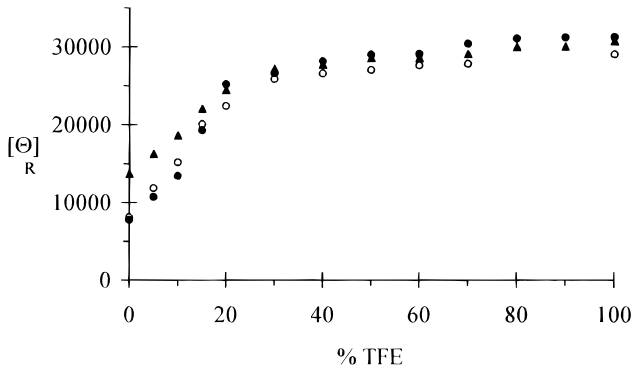

FIGURE 2: Onset of α-helix in analogs **I**−**III** on addition of TFE. Plots are of molar ellipticity at 220 nm as a function of TFE concentration in acidic aqueous solutions: analog **I** (●), analog **II** (○), and analog **III** (▲).

corresponding to seven or eight helical residues. The double-bridged analog **III** is 40% helical, corresponding to ∼13 helical residues. Thus, the induction of helix by the lactam cyclization is independent of the position of lactam in the sequence (13−17 and 26−30 are similar) and is additive in the case of analog **III**, which contains both lactam bridges.

As anticipated, CD spectra recorded with increasing TFE, a structure-inducing solvent, indicate an increase in helix content (Figure 1). More importantly, the spectra recorded in water or in the presence of <10% TFE(v/v) do not fit the isodichroic point, typical of the two-state coil−helix transition, of the spectra recorded at higher TFE concentrations. This fact and the blue shift of the negative π−π* transition band to 205 nm in water, distinctly observed in the case of analogs **I** and **II**, indicate the presence of a contribution to the optical activity attributed to a coexisting ordered conformation in addition to helix and random coil. In addition, a different TFE-induced folding pathway of the three analogs is revealed by the profiles of the plots of molar ellipticity at 220 nm versus TFE content (Figure 2). In the case of analogs **I** and **II**, an S-shaped profile is observed (more pronounced for analog **I**), while analog **III** exhibits an exponential profile. The pronounced sigmoid TFE-titration curves observed for analogs **I** and **II**, in contrast to the exponential titration curves observed for analog **III** (Figure 2), suggest that the monocyclic analogs undergo a helix nucleation process resulting in a "lag period". The folding for the bicyclic analog **III**, which contains lactam bridges at

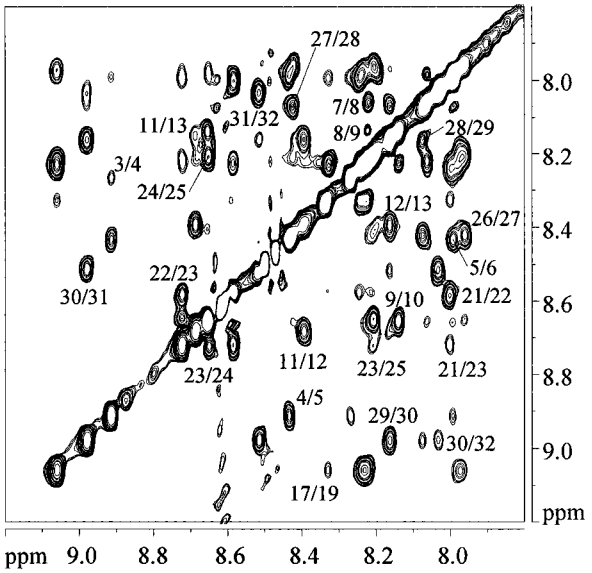

FIGURE 3: Amide region of a NOESY spectrum in 1:1 TFE-d_3/H_2O for analog **III** (concentration, 3 mM; mixing time, 200 ms; temperature, 298 K; pH ~4.5). Some of the sequential connectivities are indicated.

both the midregion and the C-terminal portion, is a linear propagation of helicity upon addition of TFE. Unlike in the monocyclic lactams, where there remains an extended linear portion in which nucleation may occur, the presence of both lactam bridges may provide the elements needed for initiation of helix formation. Interestingly, the sigmoid titration curve for the midregion-containing lactam **I** is much more pronounced than that of the C-terminal region containing lactam **II**. This may support the notion that, in the linear parent peptide, the binding domain 25−34 is *a priori* more helical and has a greater tendency to form a helix than the midregion domain (*20*−*23*). For all three analogs, the maximum helix content is reached at ~30% TFE. At a 1:1 (v/v) ratio of TFE and water, the helical content is ~80%, consistent with 26 or 27 out of the 34 residues being in a helix conformation.

NMR Measurements. The assignment of the NMR proton signals of the three peptides was achieved by standard procedures (*24*). Spin systems were assigned using DQF-COSY and TOCSY spectra; sequence-specific assignments were achieved through NOESY experiments. The assignments are reported in Tables I−III of the Supporting Information. An exemplary NOESY spectrum of analog **III** is given in Figure 3. In Figure 4, the summary of NOESY connectivities relevant for the assessment of secondary structure is reported.

From the NOE pattern [αH(*i*)−NH(*i* + 3) and αH(*i*)−*β*(*i* + 3), Figure 4A] of analog **I**, it is possible to identify a long helical segment from residue Ser^3 to Ala^{34}. There is a partial lack of helical NOEs centered around Gly^{12}-Lys^{13} [e.g., the cross-peak αH(12)−NH(15) is not present] which may be consistent with a kink or bend in the helix. Nevertheless, there are NOEs in this region consistent with a continuous helix: αH(10)−NH(14) (weak), αH(11)−NH(15) (medium), and αH(12)−*β*H(15) (strong). In addition, αH(*i*)−NH(*i* + 4) signals are uniformly present from position 5 to the end of the sequence while sequential αH−NH signals of medium intensity are present all along the sequence. The presence of an αH(*i*)−NH(*i* + 2) NOE is indicative of a 3_{10}-helix. In analog **I**, such signals appear in the N-terminal region [αH(3)−NH(5)], across the lactam bridge region [αH(15)−NH(17) and αH(19)−NH(21)], and in the C-terminal portion [αH(23)−NH(25), αH(27)−NH(29), and αH(32)−NH(34)]. A turn of a 3_{10}-helix at the end of α-helices is commonly observed in protein structures (*25*). The secondary shifts of the Hα protons, illustrated in Figure 5A, are negative for residues 7−34, with a cluster of values of less than −0.2 for residues Arg^{20}−Ile^{31}, especially indicative of an α-helix. The segment consisting of residues 7−34 corresponds to ~80% of the peptide, which is in agreement with the extent of helix estimated from the CD spectra.

For analog **II**, medium-range connectivities consistent with an α-helix [i.e., (*i*)−(*i* + 3) and (*i*)-(*i* + 4)] are observed from residue Glu^4 to residue Ala^{34}, corresponding to ~85% of the peptide. As with analog **I**, there is a distinct lack of α-helix NOEs centered about Lys^{13} (see Figure 4B), which may be attributed to a kink in the helix. There are two NOEs [i.e., αH(12)−*β*H(15) and αH(10)−NH(14)] which connect the helical segments before and after Lys^{13}. Unfortunately, some informative NOEs in this region could not be unambiguously assigned due to resonance overlap. Cross-peaks diagnostic of a 3_{10}-helix, αH(*i*)−NH(*i* + 2), appear at the ends and in the middle [αH(15)−NH(17)] of the sequence, in accordance with a structure comprising two helix stretches. The secondary shifts of the Hα protons (Figure 5B), characterized by two minima, centered around Leu^8 and Lys^{26}, are consistent with the presence of two-helix segments separated by a kink or turn.

The largest number of NOEs is observed for the double-lactam-bridged analog **III**. Similar to the single-lactam-bridged analogs, the NOEs (Figure 4C) indicate a helical region from residue 4 to 34, with distinct NOEs around Lys^{13} [i.e., αH(12)−NH(15)] absent. Interestingly, αH(*i*)−NH(*i* + 2) signals of weak intensity are equally distributed along the peptide chain, suggesting a slightly stretched helical conformation. The secondary shifts of the Hα protons are consistent with two helical stretches separated by a kink or turn (or less well-defined α-helix) centered around Gly^{12}.

Distance Geometry Calculations. Integration of the NOESY spectrum of analog **I** provided 410 constraints, 385 of which were conformationally informative (195 intra-residue and 190 inter-residue). The DG calculations produced 83 structures which fulfilled the experimental NMR data (no distance violation was larger than 0.15 Å). The data for the backbone dihedral angle order parameter (*26*), an indication of the conformational distribution, are shown in Figure 6A. The conformation is well-ordered (order parameter of >0.75) for the segment comprising residues 3−34, with the exception of two hinges, 12−13 and 17−18, located at the extremities of the lactam bridge. The low order parameter values for residue Gly^{12} and Lys^{13} are the result of two equally populated conformations: Gly^{12}(Φ −100°, Ψ −80°),Lys^{13}(Φ −180°, Ψ 90°) and Gly^{12}(Φ −30°, Ψ 0°),Lys^{13}(Φ 120°, Ψ 0°). In contrast, the low order parameters for Asp^{17} and Leu^{18} can be attributed to a spread of conformations, centered about α-helical Φ and Ψ values. The residues comprising the lactam bridge fold into a helix loop, although certainly not an α-helix; the Φ and Ψ values of Ser^{14} and Ile^{15} are well-removed from typical values [i.e., Ser^{14}(Φ −150°, Ψ 30°),Ile^{15}(Φ −110°, Ψ −90°)]. The backbone dihedral angles of Glu^4−Lys^{11} and Arg^{21}−Ala^{34} lie in the helix region of the Ramachandran map. The best structure in terms of violation of the penalty function is shown in Figure 7A. The global picture consists of a long helical segment, 4−34, containing two discontinuities at the ends of the lactam bridge.

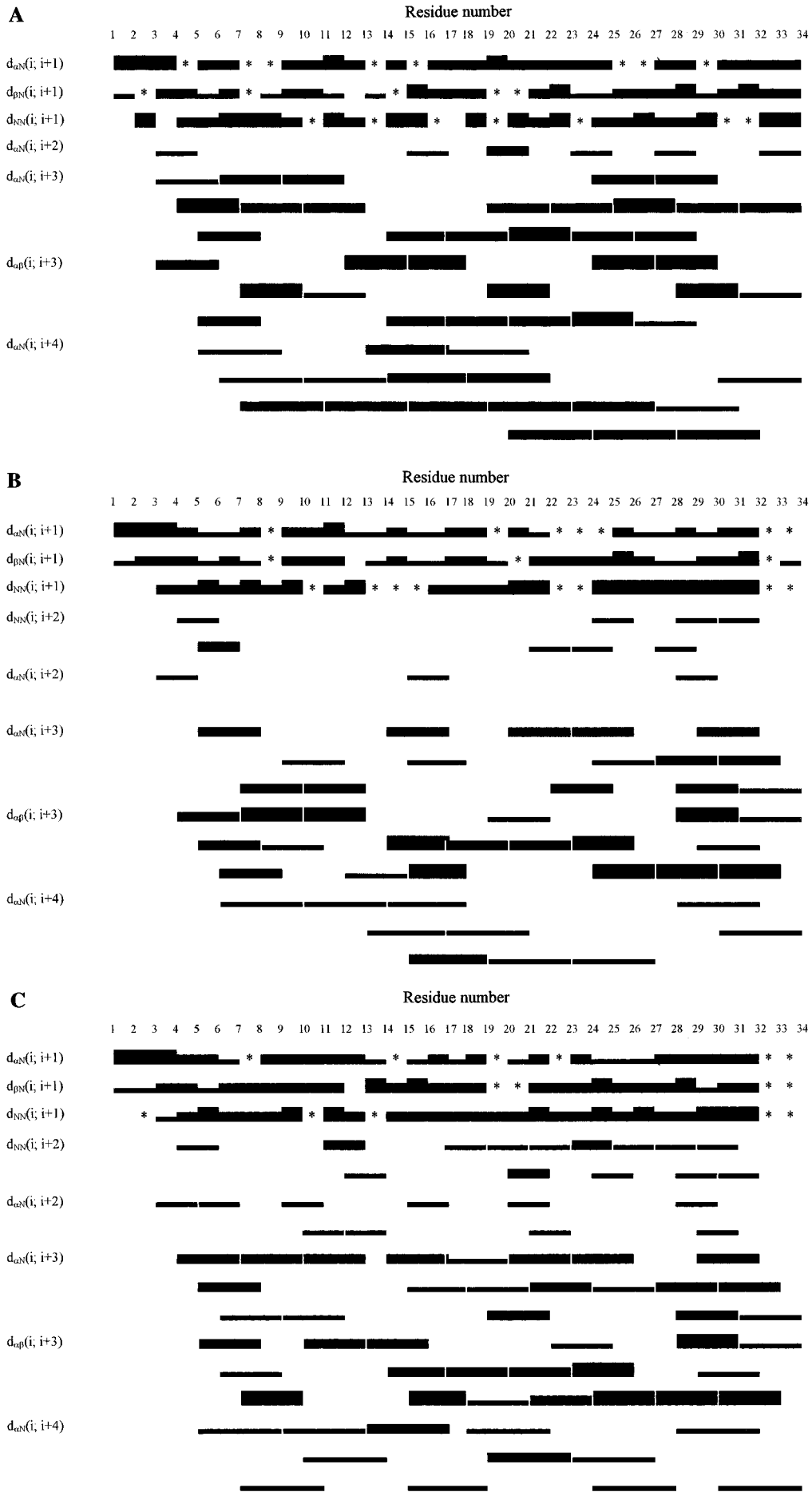

FIGURE 4: Summary of observed NOEs for (A) analog **I**, (B) analog **II**, and (C) analog **III** in 1:1 TFE-d_3/H_2O. Peaks are grouped in three classes on the basis of their integrated volumes. Asterisks indicate the likely presence of a peak which could not be confirmed because of signal overlap.

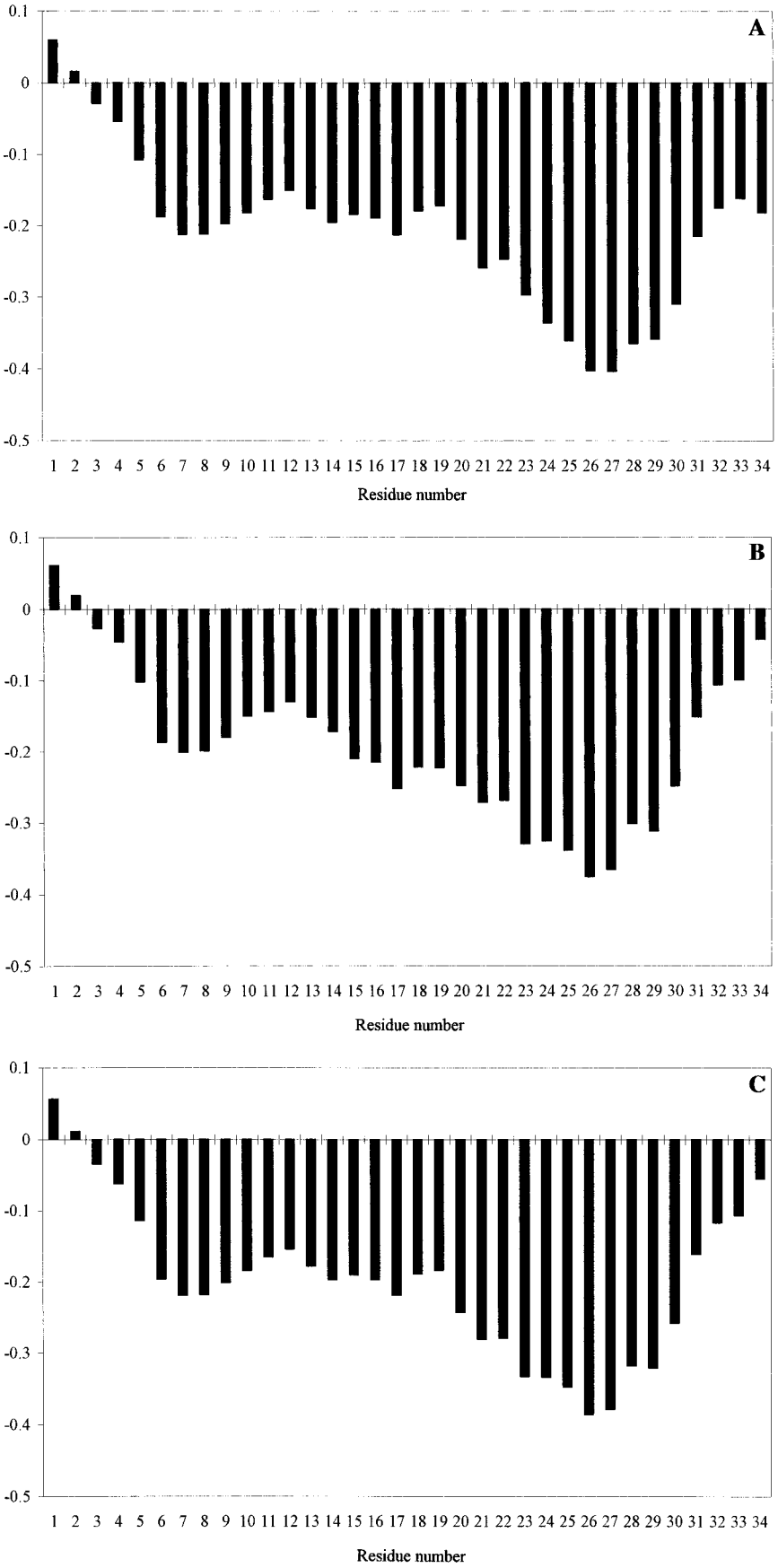

FIGURE 5: Chemical shift differences of the C^{α} protons of analog **I** (A), analog **II** (B), and analog **III** (C) in 1:1 TFE-d_3/H_2O. The chemical shifts have been averaged with the adjacent residues.

Distance geometry calculations on analog **II** were carried out using 485 distance constraints, 437 of which are conformationally informative (209 intra-residue and 228 inter-residue). The resulting 76 structures fulfilled the NOEs (there were no violations greater than 0.1 Å). The dihedral angle order parameters indicate a well-ordered structure with one region of flexibility centered about residues 13 and 14. Inspection of the Φ,Ψ maps of the 76 structures indicates

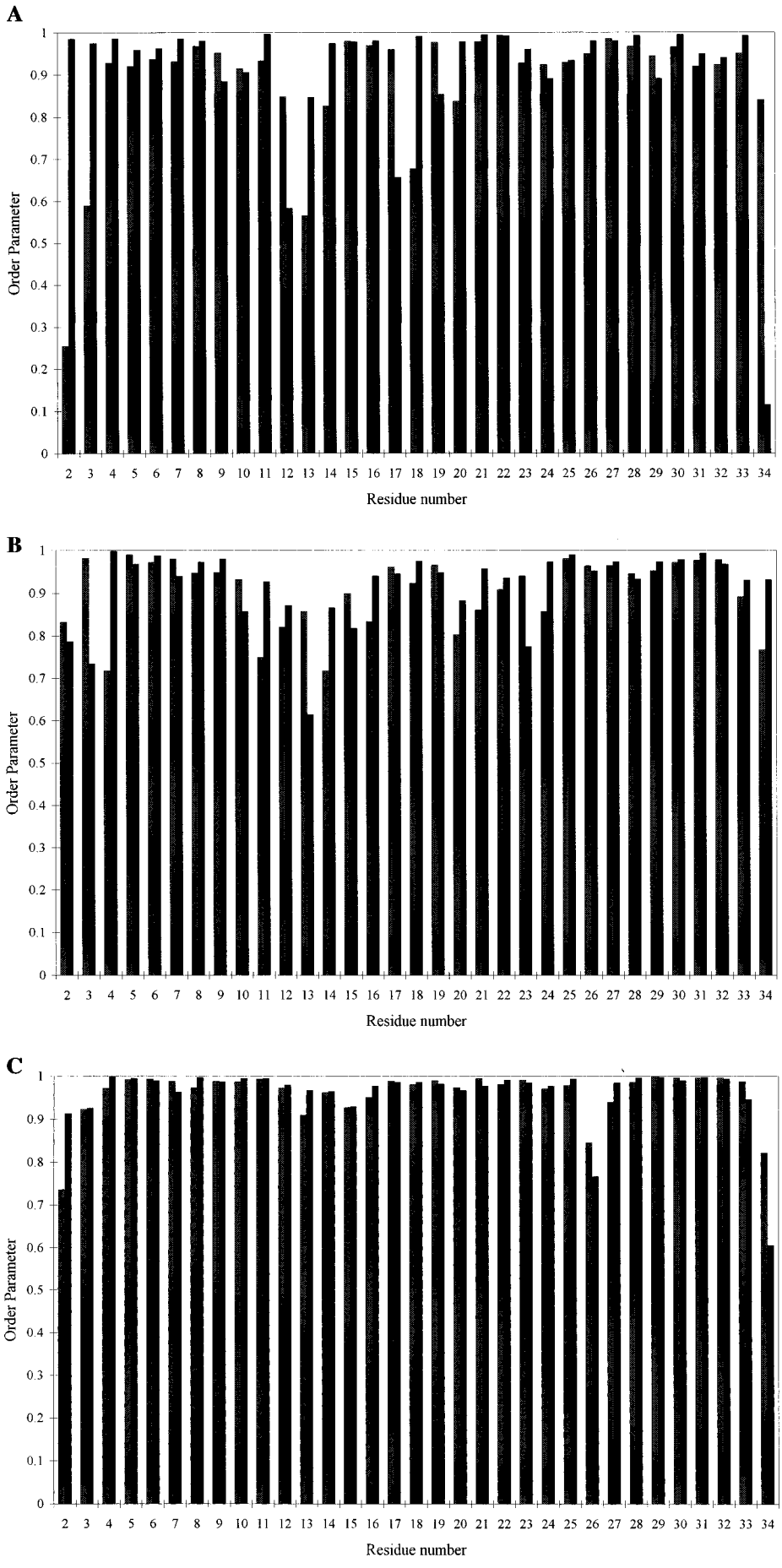

FIGURE 6: Order parameter values of the backbone Φ and Ψ dihedral angles calculated for the ensemble of structures obtained from the distance geometry calculations: (A) analog **I**, (B) analog **II**, and (C) analog **III**.

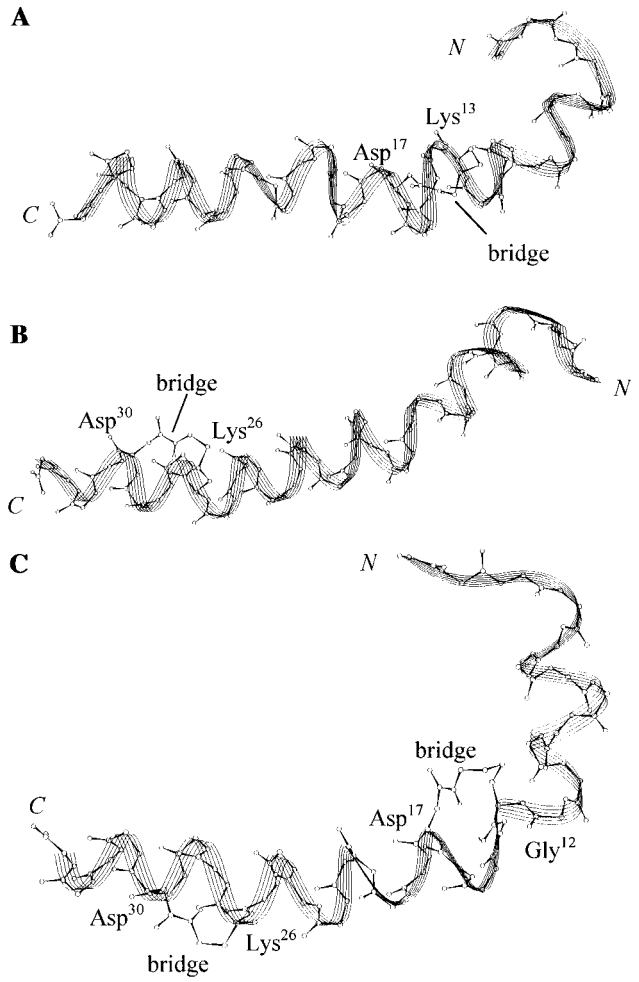

FIGURE 7: Ball-and-stick depiction of analog **I** (A), analog **II** (B), and analog **III** (C) of the DG-generated structure with the lowest penalty function.

that the low order parameters result from a great conformational freedom about Lys[13] and the presence of two families of conformations for residue Ser[14]: (Φ −60°, Ψ 0°) and (Φ −90°, Ψ −60°). The remaining residues are mainly located in the helix region with the exception of the amino acids Phe[23] and Leu[24], in which a deviation of Φ(23) and Ψ(24) dihedral angles produces a slight bend in the helical segment. The conformation with the smallest penalty violation is shown in Figure 7B.

The DG calculations of the double-bridged analog **III** made use of 512 experimental NOEs, 458 of which were informative (211 were intra-residue constraints and 247 inter-residue). The resulting 86 structures had no distance violation greater than 0.09 Å. The order parameters for the backbone dihedral angles are shown in Figure 6C. They are consistent with a well-defined structure, comprising almost the entire sequence, with some flexibility about Lys[26], generated by two populated conformations: (Φ −60°, Ψ −60°) and (Φ −120°, Ψ 20°). Residues Val[2] and Ser[3] adopt an extended conformation followed by an N-terminal helix spanning residues Glu[4]−Lys[11]. The nonhelical geometry of residue Gly[12] (Φ −150°, Ψ 0°) introduces a kink. The second helical region consists of Ser[14]−Thr[33], with two major deviations located at residue Arg[20] (Φ −120°, Ψ 0°) and Lys[26] which do not affect the general helical conformation, as illustrated in the conformation with the lowest penalty violation (shown in Figure 7C).

Molecular Dynamics Simulations. The lowest-energy structure from the DG calculations described for each of the three analogs was subjected to extensive MD simulations to further refine the conformation. The metric matrix DG method is specifically designed for exploration of conformational space which is consistent with applied experimental restraints (i.e., distance restraints derived from NOEs). Many energetic features important for conformation are ignored: Coulombic attraction of partially charged atoms or fully charged side chains, Lennard-Jones nonbonded function for atomic attraction and repulsion, and favorable rotamer populations about dihedral angles. Therefore, it is important to carry out a two-step protocol: DG for a complete searching of conformational space compatible with the NMR data followed by extensive MD simulations using explicit solvent and an all-atom force field for the development of high-resolution structures.

The MD simulations were carried out employing an explicit, full-atom representation of TFE, using previously published potential energy parameters (*19*). The use of pure TFE eliminated the use of combinatorial rules for the water−TFE interactions. In addition, the CD results, presented above, indicate no change in conformation from 50% TFE up to 100% TFE. The average and standard deviations of the backbone dihedral angles, over the last 80 ps of the simulation, are given in Table 2.

The resulting structure from the MD simulation of analog **I** can be described as two α-helical domains: Glu[4]-His[9] continuing into a turn of a 3_{10}-helix and an extended helix from Phe[22] to Thr[33]. Between these two well-defined α-helices, there is a helical-like turn consisting of residues Gln[16]−Arg[20]. Analog **II** also displays two α-helical regions: His[5]−His[9] followed by one turn of a 3_{10}-helix and Arg[21]−Leu[27] followed by two twists of a helix-like conformation. The resulting conformation of analog **III** is almost a continuous α-helix. There is a small deviation from helix in the region about residues Gln[16]−Arg[19] which leads to a slight hinge in the extended structure.

In terms of helical content, CD and NMR results agree fairly well, within 5−10%. DG and MD calculations allowed for the refinement of the structures of the three lactam-containing PTHrP analogs and for the achievement of low-energy structures which fulfil the experimental NOE constraints in the presence of an explicit representation of the TFE solution.

DISCUSSION

The conformational predominance of α-helix in PTHrP is both predicted by Chou−Fasman analysis and frequently observed by CD and NMR studies carried out in membrane-mimetic conditions and in structure-promoting solvents such as trifluoroethanol (TFE). These studies indicate that TFE produces structures similar to those observed in membrane mimetics and therefore may be suitable for the determination of membrane-bound conformations. Therefore, the prevailing hypothesis argues that α-helicity is a highly abundant conformational motif in the calciotropic-relevant PTHrP conformation. The lactam-containing PTHrP analogs **I**−**III** were designed in an attempt to stabilize and perhaps extend helical segments in either the C-terminus or the midregion of the molecule. The results presented in this study confirm that, in aqueous solution, all three analogs have enhanced helicity (22−40%) compared to the linear parent compound

Table 2: Average and Standard Deviations of the Backbone Dihedral Angles from the NOE-Restrained Molecular Dynamics Simulations in TFE[a]

		analog **I**		analog **II**		analog **III**	
residue	torsion	av	SD	av	SD	av	SD
A^1	ψ	92.8	16.6	105.9	24.7	102.2	24.4
V^2	ϕ	−144.9	8.3	−91.8	16.7	−92.1	20.1
	ψ	46.9	10.7	166.0	17.8	144.5	11.9
S^3	ϕ	−120.9	14.7	−92.5	13.0	−131.4	14.9
	ψ	166.5	7.5	−129.5	6.2	169.8	6.1
E^4	ϕ	−78.3	12.3	173.5	8.7	−57.3	7.4
	ψ	−43.7	5.6	−56.4	6.1	−35.0	6.6
H^5	ϕ	−53.5	7.7	−66.1	6.6	−69.4	8.5
	ψ	−30.2	8.7	−33.8	6.7	−19.0	9.5
Q^6	ϕ	−59.0	8.2	−53.5	8.7	−72.7	9.0
	ψ	−51.5	5.5	−42.9	6.0	−50.5	6.1
L^7	ϕ	−64.8	6.8	−62.0	7.4	−59.4	6.0
	ψ	−23.2	8.5	−21.6	7.2	−29.4	10.0
L^8	ϕ	−63.9	8.0	−61.8	8.0	−54.9	12.4
	ψ	−40.7	8.1	−52.7	5.0	−47.7	6.4
H^9	ϕ	−62.3	7.7	−57.7	6.8	−55.4	7.9
	ψ	−56.6	8.1	−30.2	7.7	−50.6	5.8
D^{10}	ϕ	−67.5	9.5	−68.0	10.4	−48.9	8.7
	ψ	−15.8	7.7	−30.5	6.5	−32.9	7.5
K^{11}	ϕ	−62.8	8.7	−84.2	8.7	−72.1	10.5
	ψ	−8.4	6.6	1.4	8.4	−33.6	9.5
G^{12}	ϕ	−95.7	6.7	−73.9	6.7	−72.5	11.5
	ψ	−62.5	5.1	−99.8	6.7	−41.7	11.3
K^{13}	ϕ	−60.7	5.6	25.9	9.3	−46.0	10.1
	ψ	0.2	7.3	−91.1	6.3	−54.7	5.9
S^{14}	ϕ	−140.7	5.8	−50.6	9.6	−47.6	6.0
	ψ	57.3	5.4	9.8	10.4	−32.6	8.7
I^{15}	ϕ	−122.2	6.5	−105.9	8.6	−81.3	7.6
	ψ	−77.5	4.8	−59.7	6.8	−54.2	6.1
Q^{16}	ϕ	−36.0	8.8	−64.3	10.8	−35.1	7.0
	ψ	−49.6	6.0	18.4	19.2	−43.6	6.6
D^{17}	ϕ	−99.2	6.6	−120.6	11.4	−82.6	8.4
	ψ	−12.6	6.9	−58.5	5.5	−42.2	6.8
L^{18}	ϕ	−49.0	5.6	−53.4	9.2	−42.0	7.6
	ψ	−60.1	5.6	−24.7	8.7	−42.9	5.9
R^{19}	ϕ	−57.9	7.0	−85.0	5.9	−77.5	7.5
	ψ	−43.0	8.8	−4.1	7.3	−13.8	7.8
R^{20}	ϕ	−88.1	7.8	−131.2	6.7	−77.1	7.3
	ψ	27.6	10.0	−63.0	5.1	−39.2	8.6
R^{21}	ϕ	−107.4	10.7	−53.3	6.1	−61.4	9.4
	ψ	−42.9	5.7	−37.9	5.4	−39.8	5.4
F^{22}	ϕ	−53.1	8.4	−59.3	5.5	−65.8	6.7
	ψ	−45.1	6.0	−55.4	5.9	−36.2	6.6
F^{23}	ϕ	−65.8	7.6	−42.3	6.9	−70.9	7.4
	ψ	−28.2	7.0	−49.8	5.6	−24.6	6.9
L^{24}	ϕ	−52.0	7.7	−63.8	7.0	−81.0	7.9
	ψ	−43.9	11.0	−25.8	6.5	−29.7	6.6
H^{25}	ϕ	−71.3	8.8	−64.0	6.9	−57.7	8.1
	ψ	−16.5	6.2	−54.1	6.4	−50.8	6.6
K^{26}	ϕ	−70.0	6.8	−60.7	8.0	−47.6	7.1
	ψ	−37.7	6.9	−49.0	5.3	−70.3	5.1
L^{27}	ϕ	−58.7	7.2	−30.8	6.5	−36.9	7.0
	ψ	−40.9	6.1	−40.1	5.2	−54.7	5.7
I^{28}	ϕ	−65.2	7.6	−80.2	6.8	−70.3	6.2
	ψ	−29.7	6.7	−41.7	7.7	−37.6	6.4
A^{29}	ϕ	−65.5	7.1	−57.6	7.3	−70.0	6.5
	ψ	−28.9	14.4	−24.0	7.7	−31.5	6.7
D^{30}	ϕ	−79.0	23.2	−93.6	7.5	−69.6	6.6
	ψ	−43.2	9.6	−23.3	5.6	−31.1	5.6
I^{31}	ϕ	−49.8	8.7	−46.7	11.9	−63.6	8.2
	ψ	−46.5	5.7	−61.7	8.8	−52.8	6.3
H^{32}	ϕ	−55.3	6.6	−91.7	8.2	−54.3	5.3
	ψ	−47.5	9.5	−2.5	8.9	−40.5	11.1
T^{33}	ϕ	−58.8	9.4	−28.8	7.3	−60.8	12.5
	ψ	−35.4	9.4	−49.0	7.0	−49.0	10.4
A^{34}	ϕ	−74.	10.5	−93.7	10.1	−68.4	11.6
	ψ	−77.4	59.0	52.4	27.4	−50.5	17.1

[a] The averages are calculated from the last 80 ps of the 120 ps simulation.

PTHrP-(1−34) in water (10−15%) (*27*). This confirms that the $(i)-(i)+4$ side chain to side chain lactamization has a helix-inducing effect.

The biologically compatible conformational constraint introduced in the mono- and bicyclic lactam-containig PTHrP agonists and antagonists makes them superior reporters of the biologically relevant bioactive conformation (*28*). We conclude, from our previous (*4*, *5*, *29*, *30*) and current studies, that bioactive PTHrP-based agonists and antagonists share a common bioactive conformation (Figures 8 and 9). This includes a relatively stable C-terminal amphiphilic helix and an N-terminal inducible helix. Both helical domains are combined by a molecular hinge centered around Arg^{19}. This particular molecular hinge plays a critical role by allowing the helices in PTHrP-derived ligands to achieve the optimal interactions with the PTH/PTHrP receptor. The distinction between the agonists and antagonists is the truncation of the activation domain (residues 1−6) from the latter which eliminates a critical agonist-mediated conformational change in the PTH/PTHrP receptor, thus disabling an intracellular signaling event.

The helical contents of lactam-containing PTHrP-derived agonists and antagonists in aqueous solution and their TFE titration profiles provide important insight on the relative stability of the two helical domains and potential interactions as well as the effect of TFE as a structure-promoting solvent.

The fact that the helix content of the bicyclic analog **III** is only 2-fold higher than that of the monocyclic analogs **I** and **II** suggests that there is no cooperative interaction between the bridged regions. The two lactams at the C-terminus and midregion have different consequences on the stabilization of α-helices. The putative major binding region at residues 25−34 displays an almost perfect α-helix in analog **I**, which contains the midregion lactam. Despite the design of analog **II**, which aimed to stabilize an already existing helix by the introduction of a C-terminal lactam bridge, we observed significant deviation from standard helical Φ,Ψ values (Table 2). Therefore, the selection of Lys(i),Asp($i+4$) may not be the optimal cyclization mode in terms of the ring size, orientation of the lactam ring, or composition of the sequence included in the lactam ring (*31*, *32*). Surprisingly, the helicity in the C-terminal lactam in analog **III** is restored; the Φ,Ψ values are very close to standard helix values in contrast with the same lactam region in analog **II** (Table 2). Therefore, there seems to be some subtle structural synergy between the midregion and the C-terminal lactams in analog **III**.

Unlike the design of the C-terminal lactam, the mid-region lactam was designed to induce or enhance the propensity of forming an α-helix. Although there is some agreement on the helical nature of the C-terminus in PTHrP-(1−34) based on Chou−Fasman analysis, CD, FTIR, and NMR studies, there is no consensus about the conformational preferences of the N-terminal domain (*33*−*37*). Introduction of an isolated midregion lactam, as in analog **I**, promotes formation of a helical structure, albeit not a perfect α-helix (Figure 7A).

In all three cyclic analogs, the long and mostly helical stretch includes residues 3−34 and differs only in the levels and sites of distortion. NOEs (Figure 4), chemical shift differences for the C^α protons (Figure 5), and order parameter values for the backbone dihedral values (Figure 6) suggest a similar perturbation (kink or bend) in the helical structure located at the midregion (Gly^{12}−Lys^{13}) for all three analogs. This perturbation is also present in DG-generated structures (Figure 7).

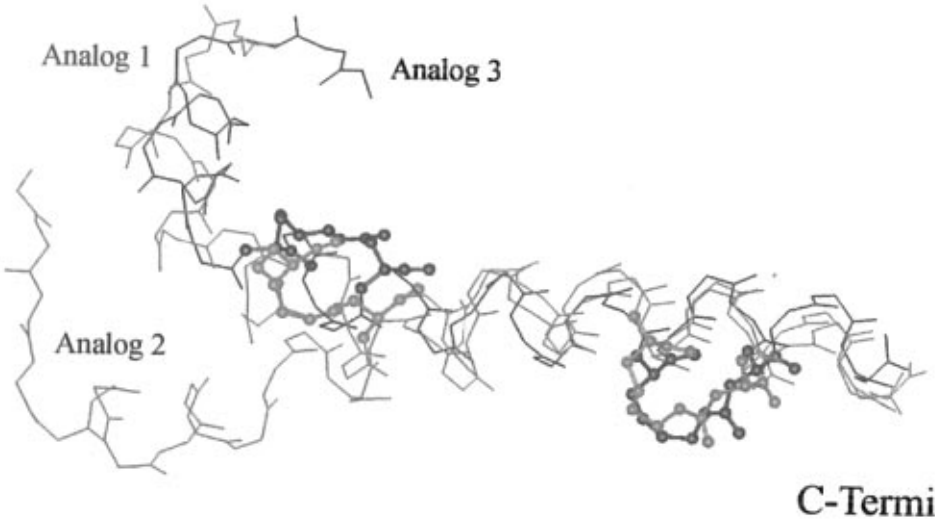

FIGURE 8: Superposition, using the heavy backbone atoms of residues 22−32, of analogs **I**−**III**. The structures were taken from the MD trajectories to illustrate the consequences of the flexible hinge centered around Arg^{19}.

The common organization into two helical domains and a hinge region centered around Gly^{12}−Lys^{13} is shared by the highly potent midregion monolactam-containing analog **I** and the dilactam-containing analog **III**, as well as by the weak agonist containing a monolactam modification at the C-terminal region (analog **II**). Therefore, our findings identify the molecular hinge centered around Arg^{19} as being essential for bioactivity. Both active agonists **I** and **III** display flexibility in approximately the same region which is not observed for the weakly active agonist **II**. DG identifies (Figure 6A, see the dip in the order parameter for these residues) a hinge region at residues Asp^{17}−Leu^{18}, located at the C-terminal end of the lactam bridge of analog **I**. The relatively high standard deviations of backbone dihedral angles extracted from the NOE-restrained MD simulations (Table 2) suggest that residues Arg^{19}−Arg^{21}, in both analogs **I** and **III**, exhibit a substantial degree of flexibility. This hinge region is missing in the structures calculated for analog **II**. Instead, the most flexible region in analog **II** is centered around residues Ser^{14}−Asp^{17} (Table 2). Additional minor sites of flexibility in analog **II** are identified at the region Arg^{19}−Leu^{24} (Figure 6B). A pronounced dip observed for residue Lys^{26} in the order parameters of analog **III** suggests a major site of flexibility located at the N-terminal end of the C-terminal lactam (Figure 6C). As will be discussed below, we attribute great significance to the presence and location of the hinge regions.

The bioactive conformational organization common to agonist **I** and **III** (Figure 8), described above, is closely related to the one observed for the highly potent antagonist [Lys^{13},Asp^{17}]PTHrP-(7−34)NH_2 in which the two helical domains, 13−18 and 20−34, are separated by a kink centered about Arg^{19} (*4*).

The bicyclic antagonist [Lys^{13},Asp^{17},Lys^{26},Asp^{30}]PTHrP-(7−34)NH_2, which has one-third of the PTH/PTHrP receptor-binding affinity of the most active monocyclic antagonist, [Lys^{13},Asp^{17}]PTHrP(7−34)NH_2, is the one which contains the most extensive and stable helix (residues 13−34) among the lactam-containing PTHrP-derived antagonists (*4*). Nevertheless, both antagonists, [Lys^{13},Asp^{17}]PTHrP-(7−34)NH_2 and [Lys^{13},Asp^{17},Lys^{26},Asp^{30}]PTHrP-(7−34)NH_2, appear to have a hinge located at Arg^{19}−Arg^{20} (Figure 9, top and bottom). In the C-terminal lactam-containing antagonist, which behaves as a weak partial agonist (*5*), this hinge was not observed (*4*) (Figure 9, middle). A comparison of the agonists and antagonists is shown in Figure 9. In the comparison, the C-terminal helices have been superimposed, illustrating the effect the hinge at residue 19 has on the topological display of the molecules. Both of the C-terminal lactam-containing analogs are extended, forming almost one continuous helical conformation (Figure 9, middle). In contrast, the biologically active analogs are kinked about residue 19 (Figure 9, top and middle). It is important to note that these are single structures taken from an MD trajectory and therefore do not display flexibility. Our intent is to illustrate the consequences of the flexibility with respect to the topological arrangement of the two helical domains.

We conclude that the lactams contribute to the stability of helical (although not always α-helical) motifs. In contrast to the cooperativity observed between midregion and C-terminal lactam domains in the antagonist series, each of the lactam-containing domains acts independently in the agonist series. The bioactive conformation in both PTHrP-derived agonists and antagonists requires well-defined midregion and C-terminal helical domains which are linked by a hinge as seen in the most active agonists (**I** and **III**) and antagonist [Lys^{13},Asp^{17}]PTHrP-(7−34)NH_2 (Figure 8). Since the folding into a helical array is initiated at the C-terminal portion of the ligands and gradually extends toward the N terminus, we envisage the following sequence of events upon binding to the PTH/PTHrP receptor. (1) Binding begins with complementary hydrophobic interactions between the amphiphilic C-terminal helical domain of the ligand (which is the principal binding domain of the ligand) and extracellular loops of the receptor. (2) Additional folding of the ligand is induced by interaction with the hydrophobic membrane (propagation of helicity can be induced by increasing TFE in an aqueous solution). (3) Formation of a midregion helical domain occurs, either cooperatively or independently from the previously formed C-terminal helical domain. (4) In the case of PTH/PTHrP agonists, a "message domain" is formed

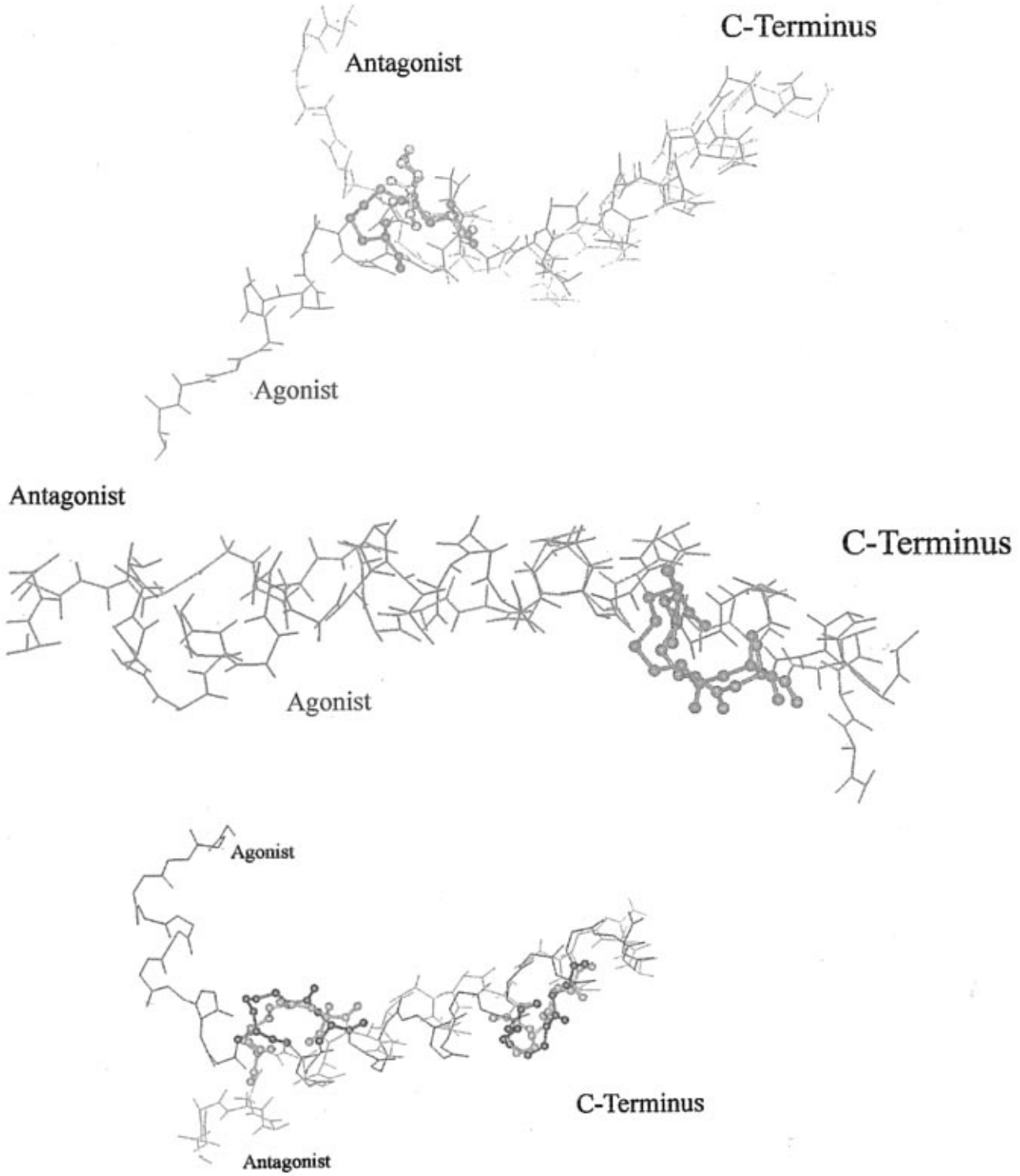

FIGURE 9: Superposition, using the heavy backbone atoms of residues 22−32, of agonists and antagonists containing the (A, top) midregion lactam, (B, middle) C-terminal region lactam, and (C, bottom) dilactam. The structures were taken from the MD trajectories to illustrate the consequences of the flexible hinge centered around Arg^{19}.

which interacts with the receptor, causing conformational change(s) in the receptor which is translated into intracellular signal transduction. In the case of PTH/PTHrP antagonists, this folding of the midregion helical domain leads, in part, to similar binding interactions. However, lacking the message domain, we observe only competitive binding.

Optimal interaction of the PTH/PTHrP receptor with the midregion helical domain (which includes the message domain, in the agonist, and is missing it in the antagonist) will take place provided a suitable hinge is present. We suggest that proper positioning of these two helical domains maximizes specific affinity for the receptor. The low biological activity of the C-terminal lactam-containing analog **II** may be attributed to the shift in register of the hinge region away from 19−22 to the 16−17 region. In other words, the long-range N-terminally-directed structuring effect induced by an isolated Lys^{26},Asp^{30} lactam bridge disrupts proper positioning of the two helical domains. The midregion lactam-containing agonist **I** does not exhibit this problem.

Instead, the isolated lactam Lys[13],Asp[17] assists the nucleation of a helical motif at the N-terminal domain and stabilizes the C-terminal helical domain, thereby conferring high binding affinity and enhanced efficacy. The mutual conformational compensatory effect generated by the combination of midregion and C-terminal lactams may be the source of the conformational properties and high biological potency of the dilactam-containing analog **III**. The deviation from perfect helicity of the midregion lactam (analog **I**) disrupts the N-terminally oriented propagation of the helicity displayed by analog **II**. This restores the flexibility at Arg[19]−Arg[20] to achieve a functional hinge and high agonistic activity.

The highly potent bicyclic lactam-bridged analog is the most rigidified PTHrP-derived agonist known to date and therefore an excellent candidate for use in elucidating the putative bioactive conformation of agonists. Our study provides additional insight regarding the importance of maintaining sufficient molecular flexibility around Arg[19] and stabilizing helical conformational motifs in order to obtain potent agonists and antagonists in the PTH/PTHrP receptor. Although we are not in a position to deduce the tertiary structure of PTH/PTHrP agonists, we have made progress in this direction.

SUPPORTING INFORMATION AVAILABLE

Proton chemical shifts of the three analogs (Tables I−III) and CD spectra of analogs **II** and **III** in TFE/water at various TFE concentrations (5 pages). Ordering information is given on any current masthead page.

REFERENCES

1. Chorev, M., and Rosenblatt, M. (1996) in *Principles of Bone Biology* (Bilezikian, J. P., Raisz, L. G., and Rodan, G. A., Eds.) pp 305−323, Academic Press, San Diego.
2. de Papp, A. E., and Stewart, A. F. (1993) *Trends Endocrinol. Metab. 4*, 181−187.
3. Goltzman, D., Hendy, G. N., and Banville, D. (1989) *Trends Endocrinol. Metab.*, 39−44.
4. Maretto, S., Mammi, S., Bissacco, E., Peggion, E., Bisello, A., Rosenblatt, M., Chorev, M., and Mierke, D. (1997) *Biochemistry 36*, 3300−3307.
5. Bisello, A., Nakamoto, C., Rosenblatt, M., and Chorev, M. (1997) *Biochemistry 36*, 3293−3299.
6. Rodan, S. B., Wesolowski, G., Ianacone, J., Tiede, M. A., and Rodan, G. (1989) *J. Endocrinol. 122*, 219−227.
7. Greenfield, N., and Fasman, G. D. (1969) *Biochemistry 8*, 4108−4116.
8. Bodenhausen, G., Vold, R. L., and Vold, R. R. (1980) *J. Magn. Reson. 37*, 93−106.
9. Rance, M., Sørensen, O. W., Bodenhausen, G., Wagner, G., Ernst, R. R., and Wüthrich, K. (1983) *Biochem. Biophys. Res. Commun. 117*, 479−485.
10. Derome, A. E., and Williamson, M. P. (1990) *J. Magn. Reson. 88*, 177−185.
11. Bax, A., and Davis, D. G. (1985) *J. Magn. Reson. 65*, 355−360.
12. Griesinger, C., Otting, G., Wüthrich, K., and Ernst, R. R. (1988) *J. Am. Chem. Soc. 110*, 7870−7872.
13. Macura, S., Huang, Y., Suter, D., and Ernst, R. R. (1980) *J. Magn. Reson. 43*, 259−281.
14. Wüthrich, K., Billeter, M., and Braun, W. (1983) *J. Mol. Biol. 169*, 949−961.
15. Havel, T. F. (1991) *Prog. Biophys. Mol. Biol. 56*, 43−78.
16. Crippen, G. M., and Havel, T. F. (1988) *Distance Geometry and Molecular Conformation*, John Wiley, New York.
17. Kaptein, R., Boelens, R., Scheek, R. M., and van Gunsteren, W. F. (1988) *Biochemistry 27*, 5389−5395.
18. Mierke, D. F., Geyer, A., and Kessler, H. (1994) *Int. J. Pept. Protein Res. 44*, 325−331.
19. De Loof, H., Nilsson, L., Rigler, R. J. (1992) *J. Am. Chem. Soc. 114*, 4028−4036.
20. Neugebauer, W., Surewucz, W. K., Gordon, H. L., Somorjai, R. L., Sung, W., and Willick, G. (1992) *Biochemistry 31*, 2056−2063.
21. Neugebauer, W., Barbier, J.-R., Sung, W. L., Whitfield, J. F., and Willick, G. E. (1995) *Biochemistry 34*, 8835−8842.
22. Klaus, W., Dieckmann, T., Wray, V., Schomburg, D., Wingender, E., and Mayer, H. (1991) *Biochemistry 30*, 6936−6942.
23. Marx, U. C., Austermann, S., Bayer, P., Aderman, K., Ejchart, A., Sticht, H., Walter, S., Schmid, F.-X., Jaenicke, R., Forssmann, W.-G., and Rösch, P. (1995) *J. Biol. Chem. 270*, 15194−15202.
24. Wüthrich, K. (1986) *NMR of Proteins and Nucleic Acids*, John Wiley, New York.
25. Barlow, D. J., and Thornton, J. M. (1988) *J. Mol. Biol. 201*, 601−619.
26. Havel, T. F. (1990) *Biopolymers 29*, 1565−1585.
27. Wray, V., Federau, T., Gronwald, W., Mayer, H., Schomburg, D., Tegge, W., and Wingender, E. (1994) *Biochemistry 33*, 1684−1693.
28. Veber, D. F., and Freidinger, R. M. (1985) *Trends Neurosci. 8*, 392−396.
29. Chorev, M., Roubini, E., McKee, R. L., Gibbons, S. W., Goldman, M. E., Caulfield, M. P., and Rosenblatt, M. (1991) *Biochemistry 30*, 5968−5974.
30. Chorev, M., Epand, R. F., Rosenblatt, M., Caulfield, M. P., and Epand, R. M. (1993) *Int. J. Pept. Protein Res. 42*, 342−345.
31. Kapurniotu, A., and Taylor J. W. (1995) *J. Med. Chem. 38*, 836−847.
32. Houston M. E. Jr., Gannon C. L., Kay C. M., and Hodges, R. S. (1995) *J. Pept. Sci. 1*, 274−281.
33. Barden, J. A., and Kemp, B. E. (1989) *Eur. J. Biochem. 184*, 379−394.
34. Chorev, M., Goldman, M. E., McKee, R. L., Roubini, E., Levy, J. J., Gay, T., Reagan, J. E., Fisher, J. E., Caporale, L. H., Golub, E. E., Caulfield, M. P., Nutt, R. F., and Rosenblatt, M. (1990) *Biochemistry 29*, 1580−1586.
35. McFarlane, D. R., McFarlane, E. F., Barden, J. A., and Kemp, B. E. (1993) *Biochim. Biophys. Acta 1162*, 187−194.
36. Ray, F. R., Barden, J. A., and Kemp, B. E. (1993) *Eur. J. Biochem. 211*, 205−211.
37. Willis, K. J. (1994) *Int. J. Pept. Protein Res. 43*, 23−28.

BI970771O